RSC Advances

PAPER

View Article Online
View Journal | View Issue

Cite this: *RSC Adv.*, 2023, **13**, 9273

Multi-color luminescence and anticounterfeiting application of upconversion nanoparticle†

Tieying Zhang,‡[a] Litao Liu,‡[b] Ru Wang,[a] Wei Zhang,[a] Xinyu Liu,[a] Chuanjun Yuan*[a] and Ruinian Hua*[a]

Received 17th November 2022
Accepted 3rd March 2023

DOI: 10.1039/d2ra07308k

rsc.li/rsc-advances

Multi-color luminescence materials are important in the illumination, solid-state three-dimensional display, information storage, biological labelling and anticounterfeiting fields. Herein, we designed a novel core–shell structure upconversion nanoparticle (UCNP) material ($NaYF_4$) with lanthanide ion doping to achieve multi-color luminescence under a single NIR excitation laser. Different from the typical single-sensitizer materials, the core–shell structure utilizes Nd^{3+}, Yb^{3+}, Tm^{3+} and Er^{3+} ions to obtain tuning of the color and brightness. The doping of Nd^{3+} ions enhances the weak color (red) light source to maintain the light color balance. Benefiting from the color adjustment of the sensitizers and the change of the core–shell coating, bright-white emission and flexible color emission from red to green, cyan and blue can be achieved *via* the diverse doped rare earth ions in a single UCNP under continuous-wave laser excitation (980 nm). Simultaneously, the emission color of the UCNPs can change with the intensity of the excitation light source and the wavelength. The bright-white emission can be used for lighting displays, and the flexible full-color emission can be applied in the anticounterfeiting and information storage fields.

Introduction

Currently, multi-color luminescence-emitting materials have attracted extensive research interest due to their wide applications in solid-state three-dimensional displays,[1] information storage,[2] biological labelling,[3,4] anticounterfeiting,[5–9] and so on. Some published studies indicate that multi-color luminescence-emitting materials have developed rapidly in recent decades, such as quantum dots (QDs),[10,11] organic materials, rare earth nanoparticles,[2,12–16] carbon dots (CDs),[17] *etc.* So far, the most common method of achieving multi-color luminescence is still color blending, in which several materials are physically mixed with separate primary emitters to produce the desired color. Nevertheless, this color-blending process unavoidably leads to color unevenness and limits the resolution. Additionally, the color modulation process for multi-color luminescence is complex, which limits its use in applications for anti-counterfeiting, information storage, *etc.* Hence, an efficient, economical, and durable multi-color luminescence source with a chemically stable host, efficient absorption, and finally, controllable emission of the three primary colors (red, green and blue) is extremely desired.

Lanthanide-doped upconversion (UC) materials have attracted wide attention because of their narrow emission band, low background signal, excellent photostability, large anti-Stokes shift and rich ladder energy levels, which can emit different wavelengths of color.[18,19] These excellent properties give them promising potential in multi-color luminescence. At present, there are two main methods to realize multi-color luminescence. One is controlling the intensities of different red–green–blue lights by doping rare earth ions into various lattices for the UC process, such as Tm^{3+}, Ho^{3+} and Yb^{3+} doped tellurite glass *via* 798 nm laser excitation,[20] Er^{3+}, Tm^{3+} and Yb^{3+} doped $NaYF_4$ glass with 980 nm laser excitation,[21] Tm^{3+}, Ho^{3+} and Yb^{3+} doped YF_3 glass under 980 nm laser excitation[22] and Er^{3+}, Pr^{3+} and Yb^{3+} doped tellurite glass under 980 nm laser excitation.[23] This is an important technique for achieving multi-color luminescence in a single material. Nevertheless, because of the high-temperature preparation and nonuniform chromaticity, the use of lanthanide-doped glass materials is limited in some fields, such as at the nanometer domain. Another technique is controlling multiple excitation light sources to achieve multi-color luminescence, such as in the cases of Nd^{3+}, Yb^{3+} doped $NaYF_4$ under continuous-wave 808 nm and pulsed 980 nm laser diode excitation,[24] and Nd^{3+}, Er^{3+} and Yb^{3+} doped $NaYF_4$ under continuous-wave 808, 980 and 1550 nm laser diode excitation.[2] Although the host material is nanoparticle, which make up the defect of glass material, this kind of multi-source white light material has high coat, stable luminous aberration and low luminous efficiency.

[a]*College of Life Science, Dalian Minzu University, Dalian, 116600, P. R. China. E-mail: rnhua@dlnu.edu.cn; ycj@dlnu.edu.cn*

[b]*School of Microelectronics, Dalian University of Technology, Dalian, 116024, China*

† Electronic supplementary information (ESI) available. See DOI: https://doi.org/10.1039/d2ra07308k

‡ Both authors contributed equally to this work.

Herein, we designed quadruply doped (Nd^{3+}, Tm^{3+}, Er^{3+} and Yb^{3+}) core–shell structure $NaYF_4$ UCNPs to obtain multi-color luminescence based on a single material under continuous-wave 980 nm laser diode excitation. Notably, the core–shell structure UCNPs can achieve multi-color luminescence at different excitation powers under 980 nm excitation. Simultaneously, the emission color of the UCNPs can be changed from white to blue with the intensity of the excitation light source. This study represents a significant improvement in the application of the nanoscale field and a simplification of the demands of multi-source excitation, which improved the performance and simplified the cost. These UCNPs with tunable multi-color luminescence present potential applications in the lighting display, anticounterfeiting and information storage fields.

Results and discussion

The $NaYF_4$ UCNPs were synthesized according to previously reported methods, and the detailed process is provided in the ESI.†[7,25] We designed a tri-layer $NaYF_4$ core–shell structure for multi-color luminescence in a step-by-step way. Schematics of the core–shell structure and energy transitions are displayed in Scheme 1. $NaYF_4$ is the host material in all layers, and the difference between each layer is the lanthanide-doped ions. As is well known, the Er^{3+} ion serves as an emitter to generate typical green and red emission due to the $^2H_{11/2}/^4S_{3/2} - {}^4I_{15/2}$ and $^4F_{9/2} - {}^4I_{15/2}$ transitions, respectively. The Tm^{3+} ion was used as the emitter that made the blue emission possible due to $^1G_4 - {}^3H_6$ transitions. Note that the Nd^{3+} ion is another emitter to generate red, green and blue emissions due to the $^2G_{7/2} - {}^4I_{13/2}$, $^4G_{9/2}/^4G_{7/2}/^2G_{7/2} - {}^4I_{9/2}$ and $^4D_{3/2} - {}^4I_{13/2}$ transitions,[12] respectively. Although the Nd^{3+} ion has great potential applications in multi-color luminescence, considering the mismatch of the energy levels of the Nd^{3+} ion with those of other lanthanide ions (Yb^{3+}, Er^{3+} and Tm^{3+}), it is difficult for the Nd^{3+} ion to sequentially absorb other lanthanide ions' pumped photons and infrared photons (980 nm) to realize multi-color luminescence. Hence, the Nd^{3+} ions in this work served as the emitter to generate red emission ($^2G_{7/2} - {}^4I_{13/2}$), which was used to improve the red emission of the UCNPs to achieve multi-color luminescence. Yb^{3+} served as a sensitizer for absorbing NIR light excitation from the 980 nm laser. Simultaneously, the core–shell structure was used for separating the rare-earth ions, which decreased the light quenching caused by non-radiative relaxation processes, and repaired the surface defects to improve the luminescence intensity.

First, based on the literature reports,[2,12,18] we designed a core doped with Er^{3+} (1%), Tm^{3+} (1%), Nd^{3+} (5%), and Yb^{3+} (20%) ions, which can emit the colors red, green and blue under 980 nm excitation. The first shell was doped with a low concentration of Tm^{3+} (0.5%) and Yb^{3+} (20%) ions to guarantee the emission intensity of the blue light and insure the efficient absorption of 980 nm photons, respectively. Additionally, the shell structure (sample 1) can repair the surface defects of the core nanoparticle and improve the emission intensity. The morphology of the core–shell structure nanoparticles was characterized using XRD and TEM. The results show that the core-$NaYF_4$ is β-$NaYF_4$, and that the size of the core is about 20 nm while the size of the core–shell structure is 25 nm, which demonstrates that a 2.5 nm shell was coated, as shown in Fig. 1a–c. The core–shell $NaYF_4$ was characterized using photoluminescence (PL) spectroscopy with different powers using a 980 nm laser. As shown in Fig. 2a, the luminescence intensity increases gradually with the increase of excitation power (0.6 W–2.6 W). Novelly, the emission light of the core–shell $NaYF_4$ changes from white to blue. The blue (455 nm) to green (545 nm) ratio gradually increases with increasing excitation power. The reason for this phenomenon is the different energy level structure of the Tm^{3+} and Er^{3+} ions, which leads to the difference in energy transfer efficiency. As shown in the energy level diagram (Fig. 2b), in the Er^{3+}–Tm^{3+}–Yb^{3+}–Nd^{3+} co-doped system under 980 nm excitation, the Yb^{3+} ion absorbs 980 nm photons and then transfers to the surrounding ions. The UC luminescence mechanism under 980 nm can be speculated from Fig. 2b.

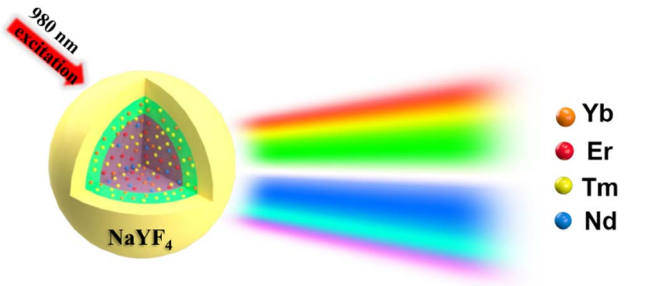

Scheme 1 Schematic of the core–shell structure and multi-color luminescence emission under 980 nm laser excitation.

The green UC emission of Er^{3+} can be achieved by the following process:[18]

$$^4I_{15/2}\ (Er) + {}^2F_{5/2}\ (Yb) \rightarrow {}^2F_{7/2}\ (Yb) + {}^4I_{11/2}\ (Er)$$

$$^4I_{11/2}\ (Er) + {}^2F_{5/2}\ (Yb) \rightarrow {}^4F_{7/2}\ (Er) + {}^2F_{7/2}\ (Yb)$$

Afterwards, non-radiative deactivation from the $^4F_{7/2}$ (Er) to the $^2H_{11/2}$ and $^4S_{3/2}$ levels result in intense green UC emission.

$$^4F_{7/2}\ (Er) \rightarrow {}^2H_{11/2}\ (Er) \rightarrow {}^4S_{3/2}\ (Er)$$

$$^2H_{11/2}\ (Er), {}^4S_{3/2}\ (Er) \rightarrow {}^4I_{15/2}\ (\text{green emission})$$

The red UC emission of Er^{3+} can be achieved *via* the above ET process as:

$$^2F_{5/2}\ (Yb) + {}^4I_{15/2}\ (Er) \rightarrow {}^2F_{7/2}\ (Yb) + {}^4I_{11/2}\ (Er)$$

Afterwards, non-radiative deactivation from the $^4I_{11/2}$ to the $^4I_{13/2}$ state occurs.

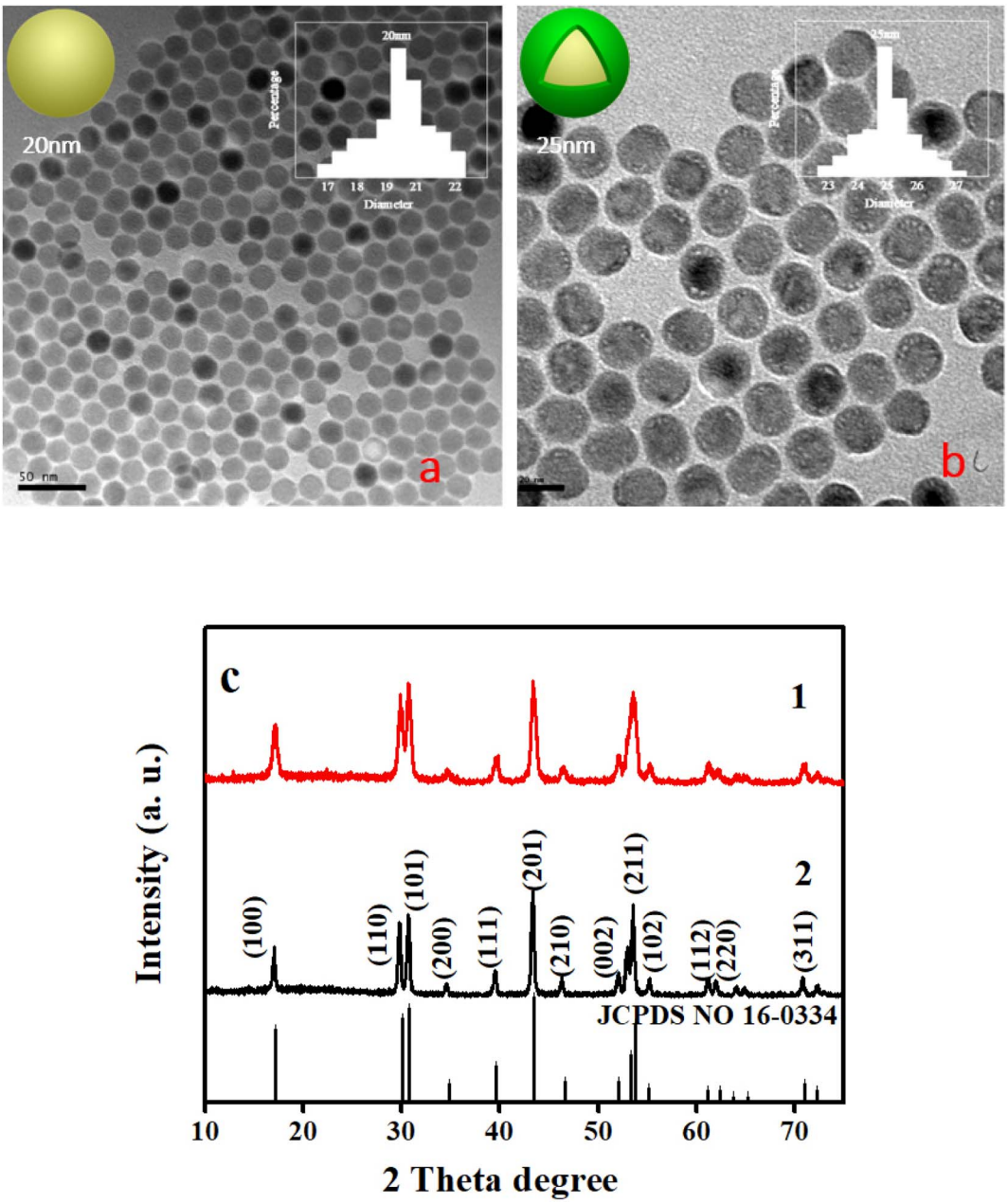

Fig. 1 Images of the morphology of $NaYF_4$: 20% Yb^{3+}, 1% Er^{3+}, 1% Tm^{3+}, 5% Nd^{3+} (a and c1) and $NaYF_4$: 20% Yb^{3+}, 1% Er^{3+}, 1% Tm^{3+}, 5% Nd^{3+}@$NaYF_4$: 20% Yb^{3+}, 0.5% Tm^{3+} (b and c2).

$$^4I_{11/2}\,(Er) \rightarrow {}^4I_{13/2}\,(Er)$$

$$^2F_{5/2}\,(Yb) + {}^4I_{13/2}\,(Er) \rightarrow {}^2F_{7/2}\,(Yb) + {}^4F_{9/2}\,(Er)$$

$$^4F_{9/2}\,(Er) \rightarrow {}^4I_{15/2}\,(\text{red emission})$$

The blue UC emission of Tm^{3+} can be achieved by the following process:[26]

$$^2F_{5/2}\,(Yb) + {}^3H_6\,(Tm) \rightarrow {}^2F_{7/2}\,(Yb) + {}^3H_5\,(Tm)$$

Afterwards, non-radiative deactivation from the $^3H_5$ to the $^3F_4$ state occurs.

$$^3H_5\,(Tm) \rightarrow {}^3F_4\,(Tm)$$

$$^2F_{5/2}\,(Yb) + {}^3F_4\,(Tm) \rightarrow {}^2F_{7/2}\,(Yb) + {}^3F_2\,(Tm)$$

$$^3F_2\,(Tm) \rightarrow {}^3H_4\,(Tm)$$

$$^2F_{5/2}\,(Yb) + {}^3H_4\,(Tm) \rightarrow {}^2F_{7/2}\,(Yb) + {}^1G_4\,(Tm)$$

$$^1G_4\,(Tm) + {}^2F_{5/2}\,(Yb) \rightarrow {}^2F_{7/2}\,(Yb) + {}^1D_2\,(Tm)$$

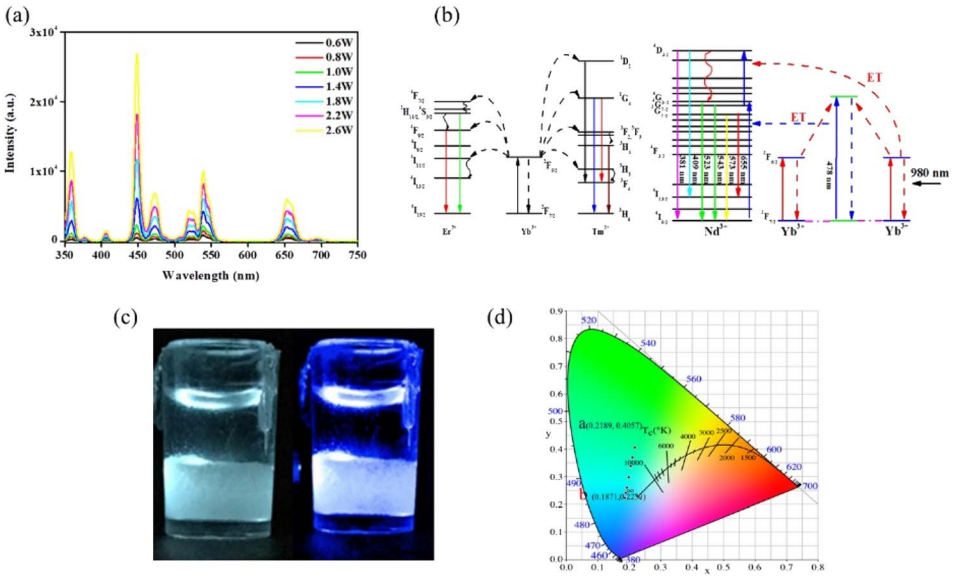

Fig. 2 PL spectra of the UNCPs (sample 1) under 980 nm excitation with different excitation powers (a); the energy level diagram of the Er, Tm, Nd and Yb dopant ions and upconversion mechanism following 980 nm laser diode excitation (b). Digital camera photographs of the UNCPs, which present white (0.6 W) and blue (2.6 W) emission under 980 nm excitation (c), and the corresponding CIE coordinates for different excitation powers (0.6–2.6 W, (d)).

$$^{1}D_2\ (Tm) \rightarrow {}^{3}F_4\ (450\ nm\ emission)$$

$$^{1}G_4\ (Tm) \rightarrow {}^{3}H_6\ (475\ nm\ emission)$$

According to the Miyakawa–Dexter theory,[12] the cooperative sensitization process of Yb^{3+}–Yb^{3+} ion pairs is dominant in the $^{4}G_{9/2}$ state in the nanoparticles under 980 nm laser excitation. Thus, the green and red UC emission of Er^{3+} can be realized by the following process:[12]

$$^{2}F_{5/2}\ (Yb) + {}^{4}G_{9/2}\ (Nd) \rightarrow {}^{4}D_{3/2}\ (Nd) + {}^{2}F_{7/2}\ (Yb)$$

Afterwards, non-radiative deactivation from the $^{4}D_{3/2}$ to the $^{4}G_{9/2}$, $^{4}G_{7/2}$ and $^{2}G_{7/2}$ states occurs.

$$^{4}D_{3/2}\ (Nd) \rightarrow {}^{4}G_{9/2}\ (Nd),\ {}^{4}G_{7/2}\ (Nd)$$

$$^{4}G_{9/2}\ (Nd),\ {}^{4}G_{7/2}\ (Nd) \rightarrow {}^{4}I_{9/2}\ (green\ emission)$$

$$^{2}G_{7/2}\ (Nd) \rightarrow {}^{4}I_{13/2}\ (red\ emission)$$

Compared with the Tm^{3+} ion, the $^{4}I_{11/2}$ energy level of the Er^{3+} ion is a better match with the Yb^{3+} ion energy level of $^{2}F_{5/2}$.[27] Hence, the Er^{3+} ion can capture more photon energy from the Yb^{3+} ion under low excitation power. The energy gained by the Er^{3+} ion gradually becomes saturated with increasing excitation power. The energy transfer to Tm^{3+} then causes the blue light to increase under high excitation power. Of course, a minority of the energy is gained by the Nd^{3+} ion to emit red and green light. Fortunately, the sample presents white light visible to the naked

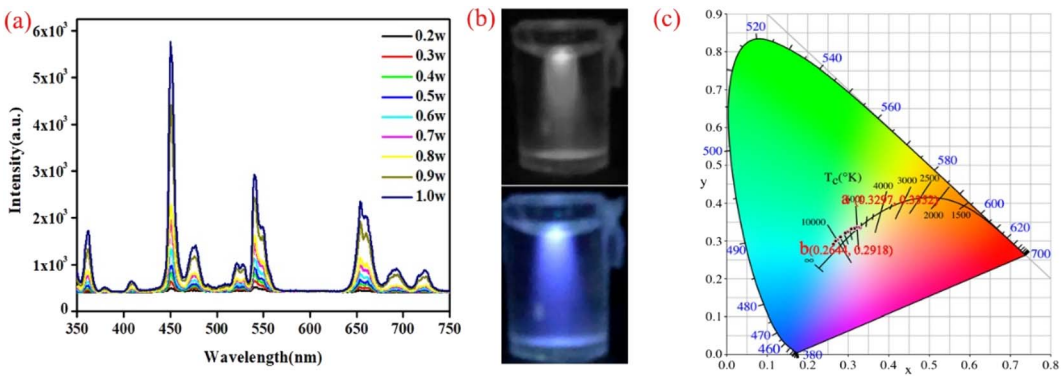

Fig. 3 PL spectra of the UNCPs (sample 2) under 980 nm excitation with different excitation powers (a). Digital camera photographs of the UNCPs, which present white (0.2 W) and blue (1 W) emission under 980 nm excitation (b) and the corresponding CIE coordinates for different excitation powers (0.2–1 W, (c)).

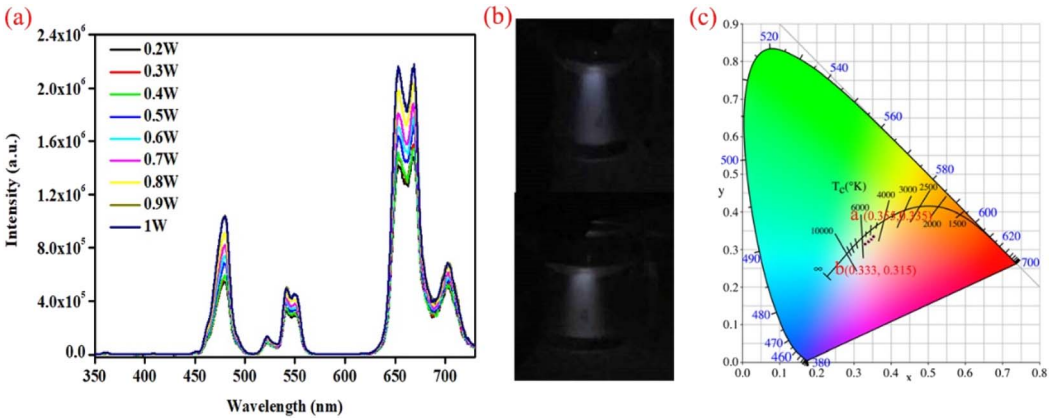

Fig. 4 PL spectra of the UNCPs (sample 3) under 980 nm excitation with different excitation powers (a). Digital camera photographs of the UNCPs, which present white emission under different excitation powers (0.2 and 1 W) of 980 nm excitation (b), and the corresponding CIE coordinates for different excitation powers (0.2–1 W, (c)).

eye under low excitation power (0.6 W), because the doping of Nd^{3+} ions enhances the weak color (red) light source to maintain the light color balance. Nevertheless, the luminescence emission of sample is gradually blue-shifted with increasing excitation power. Finally, the sample presents blue emission under a high excitation power (2.6 W), as shown in Fig. 2c. The number of photons required to populate the emitting state levels were obtained based on the laser power *vs.* emission intensity plot, which is shown in Fig. S1.† The green and red UC emissions of Er^{3+} are two-photon processes under 980 nm excitation. The blue UC emission of Tm^{3+} is a three-photon process under 980 nm excitation.

Because of psychological and physiological effects, people do not perceive colors in exactly the same way. Therefore, we used the chromaticity coordinate (CIE) for more scientific calibration. The color purity of the samples was evaluated *via* the following equation:[28,29]

$$\text{Colour purity} = \frac{\sqrt{(x - x_i)^2 + (y - y_i)^2}}{\sqrt{(x_d - x_i)^2 + (y_d - y_i)^2}}$$

where (x, y) refers to the color coordinates of the sample point, and (x_i, y_i) represent the illuminant point of the CIE Standard Source. Herein, the color coordinate of the white emission is (0.33, 0.33).[28] Also, (x_d, y_d) stands for the color coordinate of the dominant wavelength. Compared with human eye recognition, the CIE gave a different result under low excitation power (0.6 W), as shown in Fig. 2d. The result shows that the emission light is green with CIE coordinates of (0.219, 0.406) under low excitation power. Regrettably, it is not really white light under 980 nm laser excitation with a power of 0.6 W. The corresponding CIE coordinates vary from (0.219, 0.406) to (0.187, 0.223) as the excitation power is changed from 0.6 to 2.6 W. Although this cannot be used as pure white light, it has great potential for the anticounterfeiting and information storage fields.

Subsequently, a new doping system was proposed, which should satisfy the criteria of white-light emission. The new designed UCNPs had a tri-layer structure (core–shell–shell), which comprised $NaYF_4$: 30% Yb^{3+}, 0.1% Er^{3+}, 1% Tm^{3+}, 5% Nd^{3+}@$NaYF_4$: 20% Yb^{3+}, 0.5% Tm^{3+}@$NaYF_4$ (sample 2). The

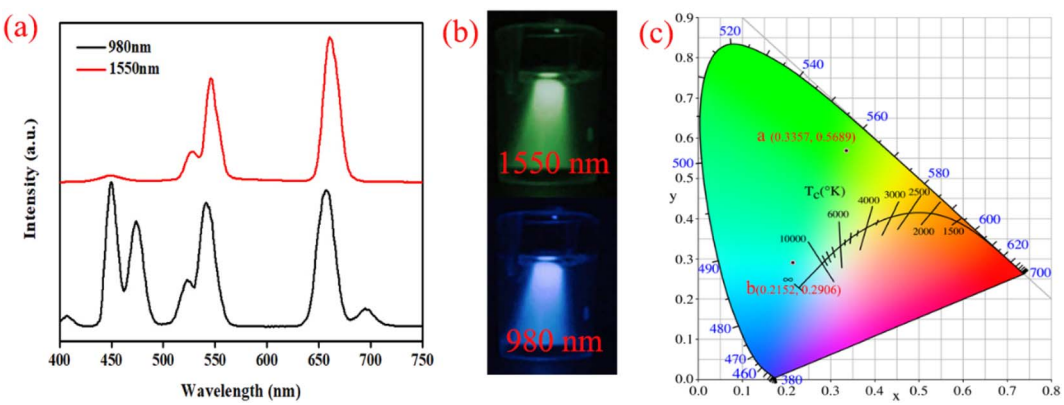

Fig. 5 PL spectra of the UNCPs (sample 4) under 980 nm with different excitation powers (a). Digital camera photographs of the UNCPs, which present green and blue emission under 1550 and 980 nm excitation, respectively (b), and the corresponding CIE coordinates for different excitation wavelengths (c).

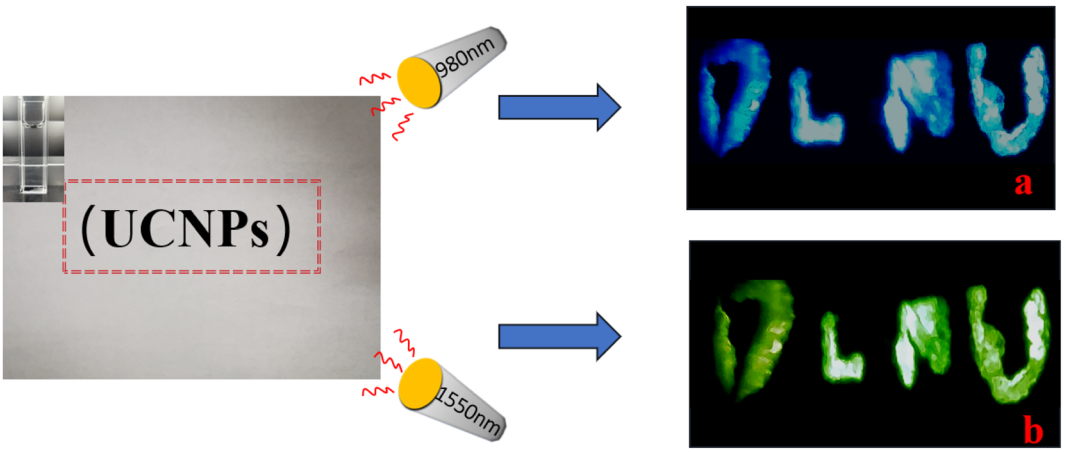

Fig. 6 Schematic diagram of the potential application using different excitation wavelengths (1550 and 980 nm).

reduction of the Er^{3+} ion concentration was intended to reduce the intensity of the green emission, and the passivation shell layer ($NaYF_4$) was intended to ensure the efficient emission of blue light, so as to emit white light at a low excitation power. The morphology of the core–shell–shell structure nanoparticles was characterized (Fig. S2 and S3†). The PL spectra were characterized under different excitation powers (0.2–1 W) using a 980 nm laser. As shown in Fig. 3a, the luminescence intensity was elevated with increasing excitation power. However, the same phenomenon occurs for the tri-layer structure UCNPs, *i.e.*, the emission of white to blue light with increasing excitation power (Fig. 3b). Novelly, compared with the core–shell structure, the white emission of the tri-layer structure UCNPs is purer. The corresponding CIE coordinates are (0.330, 0.335) at low excitation power, which approaches the standard pure white light as defined by the CIE (Fig. 3c). Hence, a sample with white emission under a low excitation power by a 980 nm laser has been synthesized. Although a white-emitting sample has been synthesized, a blue shift still occurs with increasing excitation power. In the system of sample 2, the doping concentration of Yb^{3+} ions is insufficient to provide enough photon energy to the Er^{3+} ion with increasing excitation power, which causes the blue-shift in the emitted light. Compared with the Er^{3+} ions, the Tm^{3+} ions in the shell capture photons more easily.

Hence, we continued to adjust the doping concentration ratio to achieve white-light emission at different excitation powers. The newly designed UCNPs also have a tri-layer structure, which comprises $NaYF_4$: 30% Yb^{3+}, 0.1% Er^{3+}, 0.9% Tm^{3+}, 5% Nd^{3+}@$NaYF_4$: 30% Yb^{3+}, 0.5% Tm^{3+}@$NaYF_4$ (sample 3). The Tm^{3+} ion concentration of the core layer was decreased, and the Yb^{3+} ion concentration of the shell layer was increased, which was intended to decrease the blue light emission under high excitation power and improve the transfer energies into the core to promote red emission, respectively. The morphology of the core–shell–shell structure nanoparticles was characterized (Fig. S4 and S5†). Similarly, the PL spectra were characterized with different excitation powers (0.2–1 W) under a 980 nm laser. The luminescence intensity increased with the improvement of the excitation power, but the increases in the luminescence intensity proportions of red, green and blue are almost constant, which indicates that the emitted lights are stable (Fig. 4a). Additionally, photographs appear to show pure white light under different excitation powers (Fig. 4b). The CIE coordinates were used to verify the chromaticity based on the PL spectra. The corresponding CIE coordinates vary from (0.356, 0.335) to (0.333, 0.315) as the excitation power is changed from 0.2 to 1 W (Fig. 4c), which is in the range of white light as specified by CIE. Fortunately, these UNCPs with a rare-earth-ion-co-doped core–shell structure create a new system to achieve multi-color luminescence in a single $NaYF_4$ sample.

Simultaneously, these findings provide a new way to obtain a single nanomaterial for use as a phosphor material in LEDs with multi-color luminescence, and may be applicable to data storage and luminescence coding under different excitation powers at 980 nm. Thereinto, multi-color luminescence serves as a very important light to certain technological applications, such as data storage and anticounterfeiting applications. The core–shell structure UCNPs (sample 1) have achieved this application potential, *i.e.*, they can emit different light with different excitation powers, but this requires a high excitation power to achieve.

Hence, we designed UCNPs with a new doping system ($NaYF_4$: 30% Yb^{3+}, 0.1% Er^{3+}, 1% Tm^{3+}, 10% Nd^{3+}@$NaYF_4$: 20% Yb^{3+}, 1% Tm^{3+}@$NaYF_4$, sample 4), which could achieve potential for data storage and anticounterfeiting applications using different NIR excitation lasers (980 nm and 1550 nm) under low excitation power. The morphology of the core–shell–shell structure nanoparticles was characterized (Fig. S6 and S7†). The PL spectra were obtained using different excitation wavelengths (980 nm and 1550 nm), and the corresponding CIE coordinates are (0.215, 0.291) and (0.336, 0.569), respectively, corresponding to blue and green emitted light, as shown in Fig. 5. Compared with the previous samples (1–3), the luminous mechanism of the UCNPs (sample 4) under different NIR excitation lasers is different. The Yb^{3+} ion serves as the sensitizer of the UCNPs (sample 1–3) for absorbing NIR light excitation from the 980 nm laser, and then energy transfer (ET) from Yb^{3+} to Er^{3+} and Tm^{3+}

occurs. The emission ions' (Er^{3+} and Tm^{3+}) transition to emitting levels and red, green, and blue light emission are achieved. However, the Yb^{3+} and Tm^{3+} ions cannot serve as the sensitizers of the UCNPs in sample 4 and absorb NIR light excitation from a 1550 nm laser. The Er^{3+} can absorb the photons with an energy of 1550 nm because of the energy level of $^4I_{15/2}$ and then emit the green light.

Subsequently, a simple device was constructed to demonstrate the potential applications of sample 4 in the fields of data storage and anticounterfeiting applications with different excitation wavelengths. Fig. 6 shows a schematic diagram of the potential application. First, we wrote the letters "DLNU" on a piece of A4 paper using the solution of UCNPs (sample 4), which is invisible under normal light. Then, the paper was irradiated using a 980 nm or 1550 nm laser under low excitation power after the solution had completely evaporated. The results show that the hidden letters "DLNU" show green and blue colors under 1550 nm and 980 nm excitation. Noteworthily, the colors of the hidden patterns are concealed information, which can be revealed by the excitation wavelength or power.

Conclusion

In summary, we designed quadruply doped (Nd^{3+}, Tm^{3+}, Er^{3+} and Yb^{3+}) core–shell structure $NaYF_4$ UCNPs to achieve multicolor luminescence based on a single material. The $NaYF_4$: 30% Yb^{3+}, 0.1% Er^{3+}, 0.9% Tm^{3+}, 5% Nd^{3+}@$NaYF_4$: 30% Yb^{3+}, 0.5% Tm^{3+}@$NaYF_4$ nanoparticle realizes white emission under stimulation from a single NIR laser. The corresponding CIE coordinates vary from (0.356, 0.335) to (0.333, 0.317) as the excitation power is changed from 0.2 to 1 W under 980 nm laser sensitization, which is in the standard pure white light area as defined by the CIE. Simultaneously, the structure of the sample achieves the emission of multi-color luminescence varying from red to green, cyan, blue and white *via* adjusting the concentration of activator ions (Er^{3+}: 0.1, 1 mol%; Tm^{3+}: 0.9, 1 mol%) in the sample. The mechanism of multicolor emission is the use of a dynamic energy transfer process to conduct color adjustment with different excitation powers or wavelengths. These UNCPs with a rare-earth-ion-co-doped core–shell structure create a new system to obtain multi-color luminescence in a single $NaYF_4$ sample. These findings provide a new way to control the emission of lanthanide-doped NPs to achieve tunable steady-state full-color emission, and unique optical properties to realize security anticounterfeiting designs in the field of anticounterfeiting.

Conflicts of interest

There are no conflicts to declare.

Acknowledgements

This work was supported by the Natural Science Foundation of Liaoning Province, China (Grant No. 2020-MZLH-05) and the Innovation Funds of Dalian Science and Technology Bureau (Grant No. 2021JJ12GX020).

References

1 G.-S. Yi and G.-M. Chow, *J. Mater. Chem.*, 2005, **15**, 4460.
2 X. Yin, H. Wang, Y. Tian, M. Xing, Y. Fu and X. Luo, *Nanoscale*, 2018, **10**, 9673–9678.
3 S. Han, A. Samanta, X. Xie, L. Huang, J. Peng, S. J. Park, D. B. L. Teh, Y. Choi, Y. T. Chang, A. H. All, Y. Yang, B. Xing and X. Liu, *Adv. Mater.*, 2017, **29**, 1700244.
4 L. Rao, Q. F. Meng, L. L. Bu, B. Cai, Q. Huang, Z. J. Sun, W. F. Zhang, A. Li, S. S. Guo, W. Liu, T. H. Wang and X. Z. Zhao, *ACS Appl. Mater. Interfaces*, 2017, **9**, 2159–2168.
5 X. Li, H. Chen, A. M. Kirillov, Y. Xie, C. Shan, B. Wang, C. Shi and Y. Tang, *Inorg. Chem. Front.*, 2016, **3**, 1014–1020.
6 Y. Zhang, X. Xu and B. Yan, *J. Mater. Chem. C*, 2022, **10**, 3576–3584.
7 A. J. Evangelista, M. Ivanchenko, A. F. Myers, L. N. McAnulty, G. K. M. Payne and H. Jing, *J. Mater. Chem. C*, 2020, **8**, 5692–5703.
8 Y. Chen, Q. Hu, Q. Wang, M. Yu, X. Gong, S. Li, J. Xiao, Y. Guo, G. Chen and X. Lai, *RSC Adv.*, 2020, **10**, 23410–23416.
9 B. Wang, Z. Wang, P. Mao and Y. Wang, *RSC Adv.*, 2022, **12**, 11534–11542.
10 W.-Y. Wu, M. Li, J. Lian, X. Wu, E. K. L. Yeow, M. H. Jhon and Y. Chan, *ACS Nano*, 2014, **8**, 9349–9357.
11 B. Zhou, L. Tao, Y. H. Tsang and W. Jin, *J. Mater. Chem. C*, 2013, **1**, 4313.
12 X. Wang, T. Xu, P. Cai, T. Vu and H. J. Seo, *J. Alloys Compd.*, 2017, **691**, 530–536.
13 S. Bose, M. A. Ganayee, B. Mondal, A. Baidya, S. Chennu, J. S. Mohanty and T. Pradeep, *ACS Sustainable Chem. Eng.*, 2018, **6**, 6203–6210.
14 C. Lorbeer and A.-V. Mudring, *J. Phys. Chem. C*, 2013, **117**, 12229–12238.
15 B. Wang, Z. Wang, P. Mao and Y. Wang, *RSC Adv.*, 2022, **12**, 11534–11542.
16 X. Yin, H. Wang, M. Xing, Y. Fu, Y. Tian and X. Luo, *RSC Adv.*, 2017, **7**, 50264–50268.
17 Y.-P. Sun, B. Zhou, Y. Lin, W. Wang, K. A. S. Fernando, P. Pathak, M. J. Meziani, B. A. Harruff, X. Wang, H. Wang, P. G. Luo, H. Yang, M. E. Kose, B. Chen, L. M. Veca and S.-Y. Xie, *J. Am. Chem. Soc.*, 2006, **128**, 7756–7757.
18 L. Liu, L. Cheng, B. Chen, J. Shang, X. Qi, Y. Zhu and R. Hua, *J. Alloys Compd.*, 2018, **741**, 927–936.
19 S. E. Crawford, P. R. Ohodnicki and J. P. Baltrus, *J. Mater. Chem. C*, 2020, **8**, 7975–8006.
20 N. K. Giri, D. K. Rai and S. B. Rai, *Appl. Phys. B*, 2008, **91**, 437.
21 J. Méndez-Ramos, A. C. Yanes, A. Santana-Alonso, J. Del-Castillo and V. Rodríguez, *J. Nanosci. Nanotechnol.*, 2010, **10**, 1273–1277.
22 D. Chen, Y. Wang, Y. Yu, P. Huang and F. Weng, *J. Solid State Chem.*, 2008, **181**, 2763–2767.
23 Y. Dwivedi, A. Rai and S. B. Rai, *J. Appl. Phys.*, 2008, **104**, 043509.
24 R. Deng, F. Qin, R. Chen, W. Huang, M. Hong and X. Liu, *Nat. Nanotechnol.*, 2015, **10**, 237–242.

25 W. Gao, Z. Sun, Q. Han, S. Han, X. Cheng, Y. Wang, X. Yan and J. Dong, *J. Alloys Compd.*, 2021, **857**, 157578.
26 H. Dong, L.-D. Sun and C.-H. Yan, *Chem. Soc. Rev.*, 2015, **44**, 1608–1634.
27 J.-C. Boyer, L. A. Cuccia and J. A. Capobianco, *Nano Lett.*, 2007, **7**, 847–852.
28 W. Zheng, B. Sun, Y. Li, R. Wang, T. Lei and Y. Xu, *ACS Sustainable Chem. Eng.*, 2020, **8**, 2557–2567.
29 S. Shu, Y. Wang, Y. Ke, B. Deng, R. Liu, Q. Song, J. Wang and R. Yu, *J. Alloys Compd.*, 2020, **848**, 156359.